ARTICLE

Theoretical Investigation on Reaction Mechanism and Kinetics of *M*-xylene Bicyclic Peroxy Radical with HO_2†

Zhenli Yang[a,b], Xiaofeng Tang[b], Dongdong Shu[c], Yinfeng Yang[a], Xiaoxiao Lin[b*], Weijun Zhang[b*]

a. School of Medical Informatics Engineering, Anhui University of Chinese Medicine, Hefei 230012, China
b. Anhui Institute of Optics and Fine Mechanics, Hefei Institutes of Physical Science, Chinese Academy of Sciences, Hefei 230031, China
c. Institute of Plasma Physics, Chinese Academy of Sciences, Hefei 230031, China

(Dated: Received on July 31, 2024; Accepted on September 24, 2024)

M-xylene bicyclic peroxy radical (M-BPR) is an important atmospheric intermediate formed by the oxidation of *m*-xylene, which plays an important role in the new particle formation and growth of secondary organic aerosol. In this work, the reaction mechanism, thermodynamic analysis, and kinetics of the reaction between M-BPR and HO_2 were investigated at the CCSD(T)/cc-pVDZ//B3LYP/6-311G(d,p) level of theory coupled with transition state theory. The calculated results indicate that the title reaction can occur on both singlet and triplet potential energy surfaces, and the formation of hydroperoxides and $^3O_2$ via triplet state is the main reaction channel, while the other four singlet product channels are negligible due to the higher barrier heights. Additionally, the reaction rate constants are estimated by using the transition state theory over the temperature range of 258 K to 378 K, and reaction rate constants are found to be negatively correlated with temperature. At 298 K, the total rate constant for the title reaction is 1.86×10^{-11} $cm^3 \cdot molecule^{-1} \cdot s^{-1}$. The calculated rate constants over the studied temperature range were used to fit the data and the three-parameter Arrhenius expression is obtained to be $k(T) = 4.22 \times 10^{-15} \cdot \left(\frac{T}{300}\right)^{1.44} \cdot \exp\left(\frac{2505}{T}\right)$.

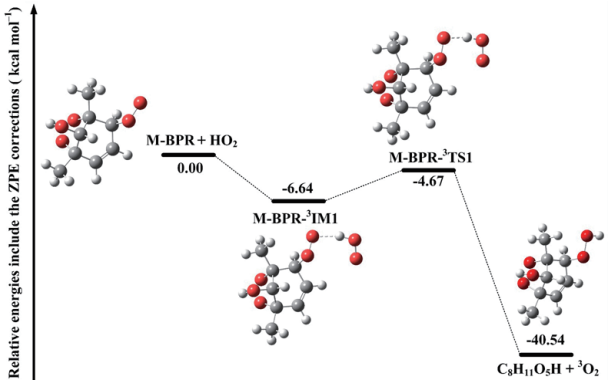

Key words: *M*-xylene, HO_2 radical, Bicyclic peroxy radical, Reaction mechanism, Transition state theory

I. INTRODUCTION

Aromatic hydrocarbons, a special class of unsaturated hydrocarbons with a benzene ring structure, are frequently appearing as the most abundant volatile organic compounds (VOC) in recent studies of the urban and regional atmospheric environments [1]. On a global scale, total emissions of aromatic hydrocarbons are on the order of 15.8 $Tg \cdot y^{-1}$, accounting for ~15% of the annual anthropogenic non-methane hydrocarbon (NMHC) budget [2–4]. Oxidation of aromatic hydrocarbons has been found to contribute significantly to the production of ozone and low volatility substances that condense in the particulate phase, which is referred to

† Part of Special Issue "In Memory of Prof. Xingxiao Ma on the occasion of his 90th Anniversary".
* Authors to whom correspondence should be addressed. E-mail: lxx1989@aiofm.ac.cn, wjzhang@aiofm.ac.cn

as secondary organic aerosol (SOA) [5–7]. Among the anthropogenic volatile organic compounds (AVOCs), aromatic hydrocarbon compounds have been recognized for a long time as the most important precursors of SOA [8, 9]. *M*-xylene is a typical aromatic hydrocarbon compound that is emitted into the atmosphere primarily from motor vehicle exhaust, the use of solvents, cigarette smoke, gasoline evaporation, and a number of industrial activities [10].

M-xylene is a relatively high abundant AVOCs in the atmosphere [11, 12]. Once emitted into the atmosphere, *m*-xylene may undergo atmospheric oxidation with the hydroxyl radical (OH), ozone (O_3), or the nitrate radical (NO_3) to form less volatile products which may undergo further reactions, leading to complex chemical composition profiles with a variety of products [13, 14]. Comparison of the reaction rate constants of *m*-xylene with these three oxidants indicates that the atmospheric photochemical reaction of *m*-xylene is essentially initiated by OH radical during the daytime [15–18]. Under atmospheric conditions, there are two reaction pathways in the reaction of *m*-xylene with OH, that is the OH addition channel with a branching ratio of 0.96 and the hydrogen abstraction channel with a ratio of 0.04 [15]. The calculations show that the OH addition to *m*-xylene initially results in four distinct structural *m*-xylene-OH adduct isomers (denoted as ortho A, ortho B, meta, and ipso, FIG. S1 in Supplementary materials, SM). ROCBS-QB3 and M06-2X predict similar branching ratios for ortho A and ortho B, that is, 0.86 and 0.12 by ROCBS-QB3 and 0.89 and 0.10 by M06-2X [15]. Obviously, formation of ortho A dominates. Most of the *m*-xylene-OH adducts undergo a preferential O_2-addition and cyclization to form peroxide-dicycloalkyl intermediates, followed by a second O_2 addition to form the *m*-xylene bicyclic peroxy radical [19, 20]. It is a complex process with several steps and several possible products. According to the research work of Fan and Zhang, there is one possible bicyclic peroxy radical (M-BPR) formed from the ortho A OH addition, and its structure is relatively stable [20]. Further, because of the high branching ratio of the ortho A that forms the *m*-xylenebicyclicperoxyradical (M-BPR), the M-BPR is mainly considered in the present investigation.

M-BPR is an important intermediate of the OH-initiated oxidation of aromatic compounds, and the fate of its bicyclic peroxy radicals depends mainly on the relative concentrations of NO, HO_2, and RO_2 [15]. The reaction of M-BPR with NO was found to yield much less bicyclic nitrate than predicted by the current mechanism, suggesting nitrate formation may be more important than SOA under high-NO_x conditions [21, 22]. However, in low-NO_x environments, the reaction of the bicyclic peroxy radical with HO_2 radicals may generate high mass, low volatility products that readily enter the particulate phase and become important components of new particle formation. *M*-xylene bicyclic peroxy radical may play an important role in the nucleation process and SOA growth, especially in low-NO_x environments, where it promotes more rapid aerosol formation and a higher aerosol yield [3, 23]. Unfortunately, in low-NO_x environments, the reaction mechanism and kinetic properties of the reaction between M-BPR and HO_2 under low-NOx conditions are currently unknown. The reactivity of aromatic bicyclic peroxy radicals toward HO_2 radicals may differ due to the effect of the O_2-bridged bicyclic group substituent.

Reaction mechanism, thermodynamic analysis and kinetics of the M-BPR + HO_2 reaction will be systematically investigated using quantum chemical methods. The structures of all reactants, intermediates, transition states and products are optimized on the B3LYP method [24] and the single-point energies of the relevant species are calculated by the CCSD(T) (coupled cluster considering single, double, and perturbative triple excitations) method [25]. Density functional theory calculation and coupled-cluster method provide insights into the reaction mechanisms and kinetic properties of *m*-xylene bicyclic peroxy radicals in the atmosphere, which not only contribute to the understanding of their environmental behaviors, but also help the assessment of their potential impacts on ecosystems.

II. COMPUTATIONAL METHOD

The quantum chemistry calculations have been employed in the geometry optimization and vibrational frequency calculations. The optimized molecular geometries of the mentioned molecules involved in the M-BPR + HO_2 reaction are performed at the B3LYP/6-311G(d,p) level of theory [26, 27]. Subsequent vibrational frequency calculations ensured that all reactants, intermediates and products are real frequencies and each transition state has only one imaginary frequency. Intrinsic reaction coordinate (IRC) calculations provide a unique connection from a given transition struc-

DOI: 10.1063/1674-0068/cjcp2407101

ture to local minima of the reactant and product sides, thus verifying that each transition state does indeed connect the associated reactants and products [28, 29].

The zero-point energy and thermodynamic corrections are calculated at the B3LYP/6-311G(d,p) level of theory and used in the calculations of the final reaction energy barrier, enthalpy and Gibbs free energy. The geometrical parameters obtained at the B3LYP/6-311G(d,p) level of theory are utilized to perform single-point energy calculations at the CCSD(T)/cc-pVDZ level of theory, which leads to an improved accuracy together with lower computational requirements. The T_1 diagnostic values in the CCSD wave function are designed to give an indication of the quality of the results that can be expected from a singles and doubles coupled-cluster calculation. For the open-shell systems, the CCSD wave function is generally considered reliable unless T_1 diagnostic value exceeds 0.044 [30–32]. The T_1 diagnostics for all electronic structures are less than the critical value of 0.044, indicating that the coupled-cluster wave functions are shown to be reliable, as shown in Table I. The optimization of the electronic structure and frequency calculations have been computed using the Gaussian 16 package [33], while the CCSD(T) single-point energy calculations were employed using the Molpro package [34, 35].

Transition state theory is a statistical rate theory based on the evaluation of the rate coefficient from the ratio of the number of thermally populated quantum states of the transition structure and the reactants [36–38]. From the framework of transition state theory, the reaction rate constants (k) for the reaction can be expressed by the following equation:

$$k = \kappa \frac{k_B T}{h} \frac{Q_{TS}}{Q_R} \exp\left(-\frac{E_{TS} - E_R}{k_B T}\right) \quad (1)$$

Here, κ is the Eckart tunneling correction and k_B is the Boltzmann constant. T is the absolute temperature and h is the Planck constant. Q_{TS} and Q_R denote the partition functions of the transition states and reactants, respectively, and E_{TS} and E_R denote the zero-point corrected energy of the transition states and reactants, respectively. Furthermore, the barrier heights are the energy differences between the reactants and transition states that determine the rate constants in transition state theory. The partition functions of the reactants and transition states were obtained at the B3LYP/6-311G(d,p) level of theory, whereas the energies in the expression were calculated by the CCSD(T)/cc-pVDZ//B3LYP/6-311G(d,p) level of theory. The rate constants were evaluated in the TheRate (Theoretical Rate) program using conventional transition state theory with Eckart tunneling correction [39, 40].

TABLE I T_1 diagnostic values for the stable structure of the M-BPR+HO_2 reaction.

Molecule	T_1	Molecule	T_1
M-BPR	0.021	$C_8H_{11}O_4H$	0.012
M-BPR-^{3}IM1	0.026	M-BPR-IM3	0.015
M-BPR-^{3}TS1	0.029	M-BPR-TS4	0.021
$C_8H_{11}O_5H$	0.013	$C_8H_{10}O_4$	0.015
M-BPR-TS2	0.026	M-BPR-IM4	0.015
M-BPR-IM2	0.015	M-BPR-TS5	0.019
M-BPR-TS3	0.027	HO_3H	0.015

III. RESULTS AND DISCUSSION

The schematic of the various routes of the M-BPR+HO_2 reaction is summarized in FIG. 1. The potential energy surfaces and optimized conFIGurations are shown in FIGs. 2 and 3 respectively. The relative energies ($\Delta(E$+ZPE) and ΔE_{298K}), entropies (ΔH_{298K}), and Gibbs free energies (ΔG_{298K}) are obtained by adding the single-point energies obtained by the CCSD(T) method to the corresponding energy corrections calculated by the B3LYP method, and these energy values have been summarized in Table II. To evaluate the importance of the different pathways, we have calculated rate constants for the five distinct pathways on the basis of the structures determined by the B3LYP method and the energy information determined by the CCSD(T) method using transition state theory. The Arrhenius plot of the total rate constants for M-BPR+HO_2 is shown in FIG. 4 and the calculated total rate constants are fitted to the three-parameter Arrhenius equation.

A. Mechanism of the M-BPR + HO_2 reaction

1. Reaction mechanism on triplet PES

Triplet potential energy surface calculations indicate that there is a possible reaction pathway that generates the products hydroperoxides $C_8H_{11}O_5H$ and oxygen molecules $^3O_2$ via the pre-reaction complex M-BPR-^{3}IM1 and the transition state M-BPR-^{3}TS1. The process is a hydrogen abstraction reaction, where the hy-

DOI: 10.1063/1674-0068/cjcp2407101

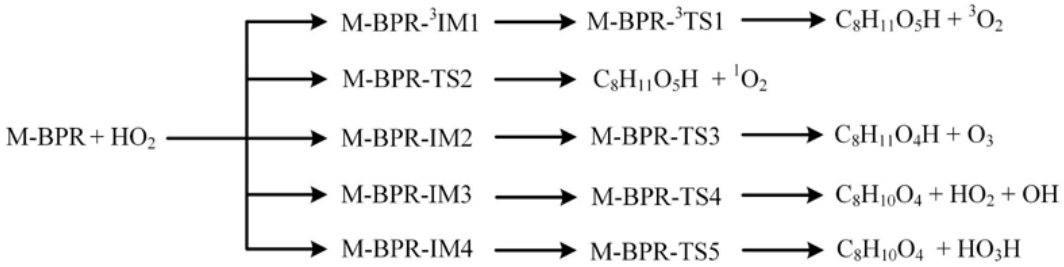

FIG. 1 The schematic reaction pathway of M-BPR+HO_2 reaction.

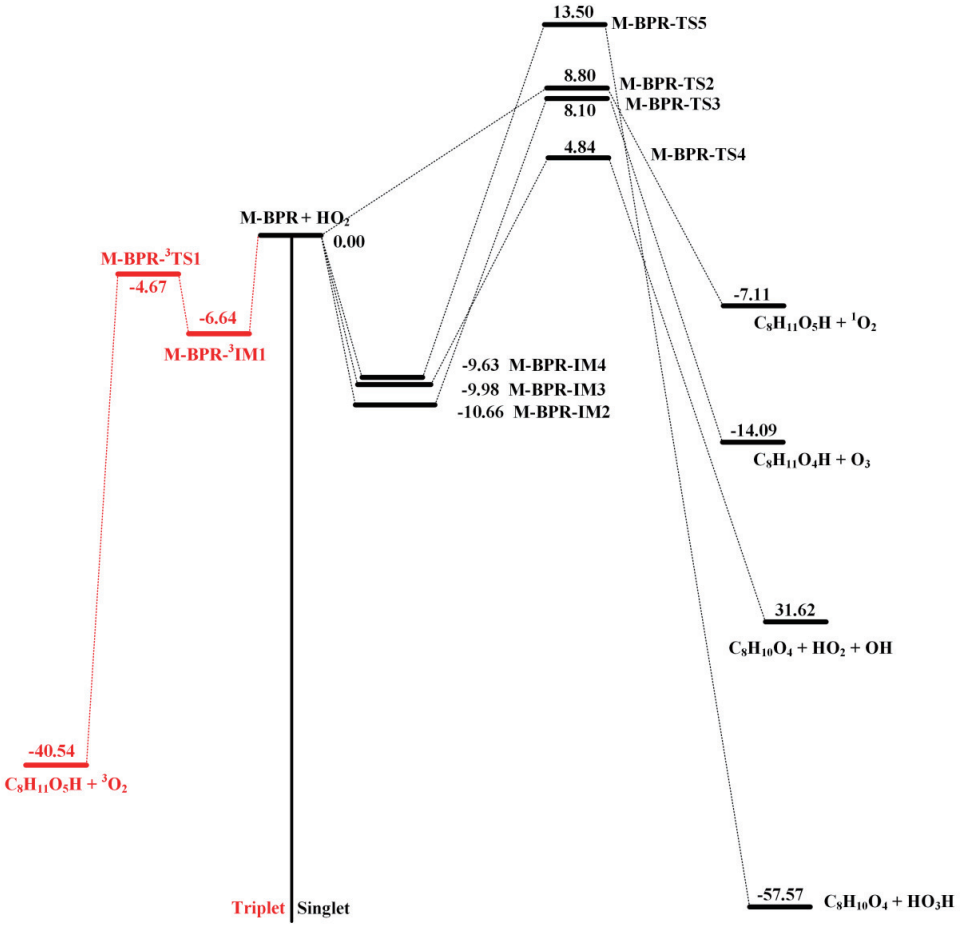

FIG. 2 The potential energy surfaces of the M-BPR+HO_2 reaction computed at the CCSD(T)/cc-pVDZ//B3LYP/6-311G(d,p) level of theory on both the singlet and triplet potential energy surfaces. Relative energies include the ZPE corrections. The triplet reaction pathways are depicted in red, and the singlet reaction pathways are depicted in black for clarity. Energies are in units of kcal/mol.

drogen atom (H1) on the HO_2 radical is transferred to the oxygen atom (O_2) at the end of M-BPR to form $C_8H_{11}O_5H$ and $^3O_2$.

The M-BPR-^{3}IM1 binding energy is –6.64 kcal/mol relative to the M-BPR + HO_2 reactants. There is a hydrogen bonding interaction in M-BPR-^{3}IM1, where the hydrogen atom of HO_2 and the oxygen atom at the end of M-BPR form a hydrogen bond with a bond length of 1.773 Å. A hydrogen bond is formed between a hydrogen atom of HO_2 and an oxygen atom at the end of M-BPR.

As shown in FIG. 3, the equilibrium structure of M-BPR-^{3}TS1 contains a broken H1–O3 and a formed H1–O2 bond, which have bond lengths of 1.032 and 1.494 Å. Compared to the H–O bond in the HO_2 radical, the length of the broken H–O bond is only slightly longer by 0.057 Å, whereas the formed H1–O2 bond is about 0.279 Å shorter than the corresponding bond length in M-BPR-^{3}IM1. Both M-BPR-^{3}IM1 and M-BPR-^{3}TS1 are nearly linear molecules with bond angles

DOI: 10.1063/1674-0068/cjcp2407101

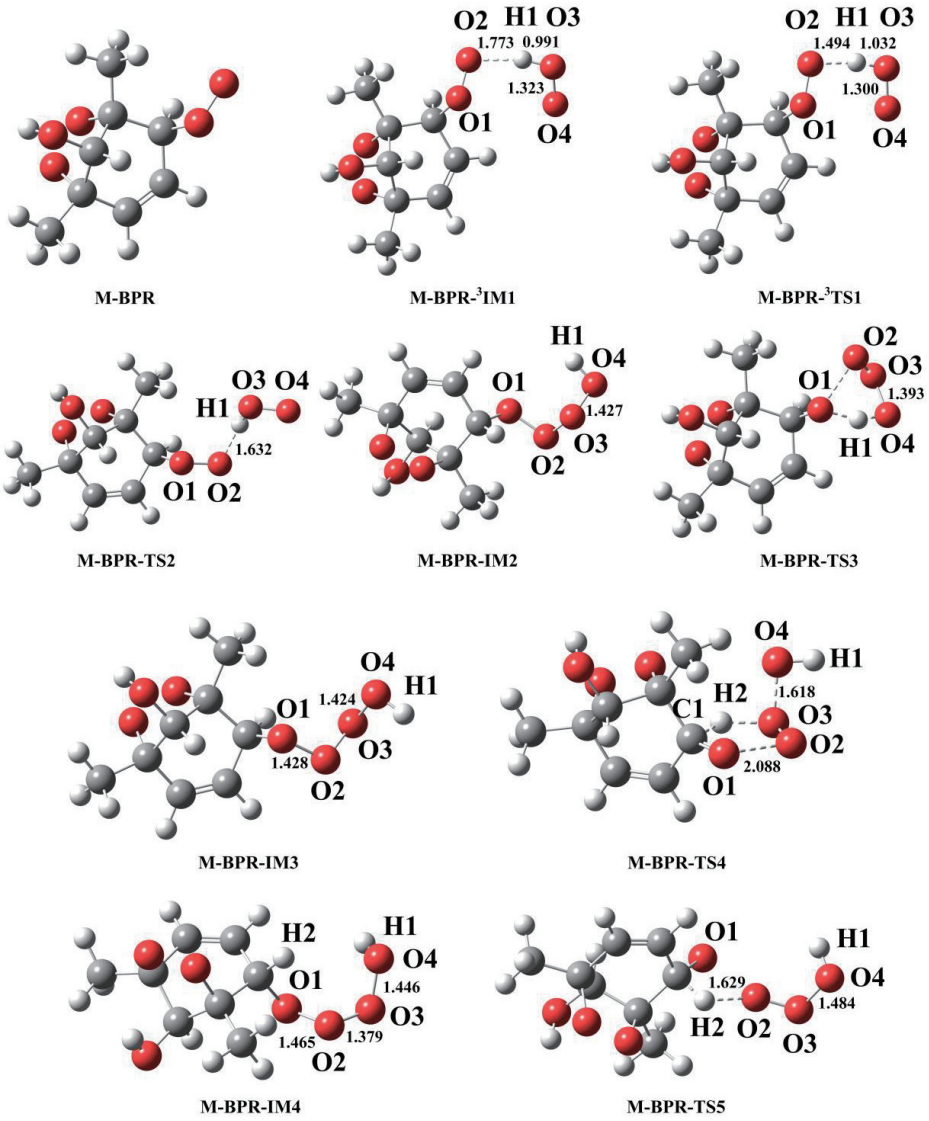

FIG. 3 Selected geometric structures of the reactants, intermediates and transition states of M-BPR+HO_2 reaction computed at the B3LYP/6-311G(d,p) level of theory on both the singlet and triplet potential energy surfaces. Bond distances are given in angstroms.

O2···H1···O3 of 161.89° and 166.02°, respectively. The energy barrier of M-BPR-^{3}TS1 is −4.67 kcal/mol (Table II).

2. Reaction mechanism on singlet PES

Computations show that the M-BPR + HO_2 reaction has four distinct product channels on the potential energy surface of singlet state, namely $C_8H_{11}O_5H + {}^1O_2$, $C_8H_{11}O_4H + O_3$, $C_8H_{10}O_4 + HO_2 + OH$ and $C_8H_{10}O_4 + HO_3H$. The reactants M-BPR + HO_2 give rise to the products $C_8H_{11}O_5H + {}^1O_2$ by way of only one transition state M-BPR-TS2 (FIG. 2). This pathway is a direct hydrogen abstraction reaction, in which the hydrogen atom H1 of the HO_2 radical is directly transferred to the oxygen atom O2 at the end of the M-BPR, and the products are produced without undergoing any pre-reaction complexes or post-reaction complexes. The theoretically calculated M-BPR-TS2 energy is 8.80 kcal/mol higher than that of the reactants. The hydrogen abstraction reaction of this pathway differs from that of the triplet state in three ways. Firstly, the direct hydrogen abstraction reaction on the potential energy surface of the singlet state generates the products $C_8H_{11}O_5H$ and ${}^1O_2$ through the transition state M-BPR-TS2 alone, whereas the triplet state also passes through the pre-reaction complex M-BPR-^{3}IM1 and the transition state M-BPR-^{3}TS1 before generating the products $C_8H_{11}O_5H$ and ${}^3O_2$. Secondly, the transition states M-

DOI: 10.1063/1674-0068/cjcp2407101

TABLE II Relative energies ($\Delta(E+\mathrm{ZPE})$ and $\Delta E_{298\mathrm{K}}$), reaction enthalpies ($\Delta H_{298\mathrm{K}}$), Gibbs free energies ($\Delta G_{298\mathrm{K}}$) involved in M-BPR+HO_2 reaction. Energy values are given in kcal/mol.

Compound	$\Delta(E+\mathrm{ZPE})$	$\Delta E_{298\mathrm{K}}$	$\Delta H_{298\mathrm{K}}$	$\Delta G_{298\mathrm{K}}$
M-BPR+HO_2	0.00	0.00	0.00	0.00
M-BPR-^{3}IM1	−6.64	−5.95	−6.54	2.09
M-BPR-^{3}TS1	−4.67	−4.63	−5.22	5.71
$C_8H_{11}O_5H+{}^3O_2$	−38.19	−38.20	−38.20	−36.41
M-BPR-TS2	8.80	9.00	8.41	19.37
$C_8H_{11}O_5H+{}^1O_2$	−7.11	−7.11	−7.11	−4.73
M-BPR-IM2	−10.66	−10.84	−11.43	1.29
M-BPR-TS3	8.10	7.64	7.04	20.36
$C_8H_{11}O_4H+O_3$	−14.09	−14.52	−9.81	−13.08
M-BPR-IM3	−9.98	−10.10	−10.69	1.75
M-BPR-TS4	4.84	4.78	4.18	17.14
$C_8H_{10}O_4+HO_2+OH$	−31.62	−31.00	−30.41	−40.43
M-BPR-IM4	−9.63	−9.20	−10.38	2.25
M-BPR-TS5	13.50	14.09	12.91	25.07
$C_8H_{10}O_4+HO_3H$	−57.57	−56.67	−57.85	−57.40

BPR-TS2 and M-BPR-^{3}TS1 have structural differences, for example, the bond angles O2···H1···O3 of the two are 109.87° and 166.02°, respectively. Thirdly, the energy barriers of M-BPR-TS2 and M-BPR-^{3}TS1 are very different, with the former being 13.47 kcal/mol higher than the latter.

In addition to the direct hydrogen abstraction mechanism described above, there is also an addition-elimination mechanism on the singlet potential energy surface. The other three reaction pathways in the singlet potential energy surface proceed through the addition-elimination mechanism. The reaction pathway that generates $C_8H_{11}O_4H+O_3$ has a high energy barrier and is exothermic. The structures of M-BPR-IM2 and M-BPR-TS3 are shown in FIG. 3. The M-BPR-IM2 structure is generated by combining the O1–O2 bond of M-BPR with the O3–O4 bond of HO_2. This structure has four oxygen atoms connected to form three oxygen–oxygen bonds, each bond with a length of approximately 1.4 Å. Relative to the reactants M-BPR+HO_2, the binding energy of M-BPR-IM2 is −10.66 kcal/mol. M-BPR-TS3 is a five-membered ring structure in which the O1–O2, O2–O3, O3–O4, O4–H1, and H1–O1 bonds have bond lengths of 2.071, 1.267, 1.393, 1.158, and 1.313 Å, respectively. The energy barrier of M-BPR-TS3 is up to 8.10 kcal/mol. The product channel $C_8H_{11}O_4H+O_3$ has a higher energy barrier and is less likely to occur in comparison to the other reaction pathways.

Through the pre-reaction complex M-BPR-IM3, M-BPR+HO_2 may form the transition state M-BPR-TS4. Calculations show that the structural information of M-BPR-IM3 is similar to that of M-BPR-IM2, which is also formed by the combination of the O1–O2 bond of M-BPR and the O3–O4 bond of HO_2. M-BPR-IM3 has three O–O bonds with a bond length of about 1.4 Å. The energy difference between the two is small (−9.98 *vs.* −10.66 kcal/mol). The energy barrier of M-BPR-TS4 is 4.84 kcal/mol, which is the lowest on the singlet state and is still 9.51 kcal/mol higher than that of the triplet reaction channel M-BPR-^{3}TS1. In the electronic structure of M-BPR-TS4, the H2 atom is transferred from C1 to O3, while O1–O2 and O3–O4 bonds are broken to form HO_2 and OH radicals. More interestingly, since HO_2 radicals are present before and after the reaction, the reaction pathway formed by $C_8H_{10}O_4+HO_2+OH$ can be viewed as a process of dissociation of HO_2 acting as a catalyst for M-BPR.

The last reaction path on the singlet state potential energy surface is M-BPR+HO_2 → M-BPR-IM4 → M-BPR-TS5 → $C_8H_{10}O_4+HO_3H$, which has a high reaction energy barrier. The binding energy of the pre-reaction complex M-BPR-IM4 is –9.63 kcal/mol, which is a small difference from the binding energies of M-BPR-IM2 and M-BPR-IM3. It is more interesting to note that the formation process and structure of M-BPR-IM4 is relatively similar to both M-BPR-IM2 and M-BPR-IM3. For the reactants M-BPR+HO_2, the M-BPR-TS5 energy barrier is 13.50 kcal/mol. This reaction pathway has a high energy barrier and is also the most exothermic on the triplet and singlet potential energy surfaces.

B. Kinetic analysis of the M-BPR + HO_2 reaction

The rate constants for the different product channels of the M-BPR+HO_2 reaction are given in Table III. k_{Total} ($k_{\mathrm{Total}}=k_{^3\mathrm{TS1}}+k_{\mathrm{TS2}}+k_{\mathrm{TS3}}+k_{\mathrm{TS4}}+k_{\mathrm{TS5}}$) are the total rate constants for the reaction, $k_{^3\mathrm{TS1}}$, k_{TS2}, k_{TS3}, k_{TS4} and k_{TS5} denote the rate constants of product channels $C_8H_{11}O_5H+{}^3O_2$, $C_8H_{11}O_5H+{}^1O_2$, $C_8H_{11}O_4H+O_3$, $C_8H_{10}O_4+HO_2+$ OH, and $C_8H_{10}O_4+HO_3H$, respectively. At 258–378 K, the rate constants for the triplet state reaction show a significant negative correlation with temperature, whereas the singlet state reactions are all positively cor-

DOI: 10.1063/1674-0068/cjcp2407101

TABLE III The theoretical rate constants within the temperature range 258–378 K for the M-BPR+HO_2 reaction at CCSD(T)/cc-pVDZ//B3LYP/6-311G(d,p) level of theory ($cm^3 \cdot molecule^{-1} \cdot s^{-1}$).

T /K	$k_{^3TS1}$	k_{TS2}	k_{TS3}	k_{TS4}	k_{TS5}	k_{Total}
258	5.59×10^{-11}	1.98×10^{-22}	1.96×10^{-21}	3.10×10^{-20}	3.26×10^{-27}	5.59×10^{-11}
278	3.08×10^{-11}	7.16×10^{-22}	2.65×10^{-21}	6.02×10^{-20}	2.27×10^{-26}	3.08×10^{-11}
298	1.86×10^{-11}	2.21×10^{-21}	3.98×10^{-21}	1.09×10^{-19}	1.23×10^{-25}	1.86×10^{-11}
318	1.21×10^{-11}	5.99×10^{-21}	6.28×10^{-21}	1.86×10^{-19}	5.46×10^{-25}	1.21×10^{-11}
338	8.33×10^{-12}	1.46×10^{-20}	1.00×10^{-20}	3.01×10^{-19}	2.05×10^{-24}	8.33×10^{-12}
358	6.03×10^{-12}	3.24×10^{-20}	1.59×10^{-20}	4.67×10^{-19}	6.72×10^{-24}	6.03×10^{-12}
378	4.55×10^{-12}	6.68×10^{-20}	2.48×10^{-20}	7.00×10^{-19}	1.96×10^{-23}	4.55×10^{-12}

related with temperature. Moreover, the rate constants of the triplet state reactions are at least seven orders of magnitude higher than those of the singlet state reactions, so that the total rate constants are mainly determined by the triplet state reaction. And the total rate constants also have a negative temperature effect as shown in Table III. Our study show that the total rate constant for the M-BPR+HO_2 reaction was 1.86×10^{-11} $cm^3 \cdot molecule^{-1} \cdot s^{-1}$ at 298 K, which is close to the rate constant (2.3×10^{-11} $cm^3 \cdot molecule^{-1} \cdot s^{-1}$) derived from the MCM v3.1. Under low-NO_x conditions, the reaction of M-BPR with HO_2 radical is competitive with other biomolecular reactions. For example, the rate constant of aromatic bicyclic peroxy radical+NO is around 10^{-12} $cm^3 \cdot molecule^{-1} \cdot s^{-1}$ [41], thus the reaction of M-BPR with HO_2 plays a larger role and makes a contribution to radical chain termination leading to the production of the hydroperoxide species (ROOH). The low-volatility organic hydroperoxides can condense onto aerosol surfaces to produce atmospheric secondary organic aerosol (SOA). This study provides basic kinetic parameter for atmospheric model studies, helping to access the formation of SOA especially under low NO_x conditions.

In the temperature range investigated, the triplet pathway for the formation of bicyclic hydroperoxide ($C_8H_{11}O_5H$)+$^3O_2$ is the main reaction channel of the M-BPR+HO_2 reaction, while the singlet pathways are to be of minor importance. The conclusion of a high yield of hydroperoxides from the reaction with HO_2 radical is in consistence with the results of a large number of other similar studies [15, 42]. For example, Birdsall and Elrod directly observed the bicyclic hydroperoxide product in experiments involving *m*-xylene bicyclic peroxy radical reacting with HO_2 [43]. And these findings have recently been confirmed in a study by He and his colleagues [21]. Hydroperoxides are thought to play an important role in the formation of secondary organic aerosol and can be used as indicators of the oxidizing capacity of the troposphere [44, 45]. Furthermore, meteorological parameters such as temperature, pressure, relative humidity and solar insolation are very important for controlling hydroperoxide production and loss [46].

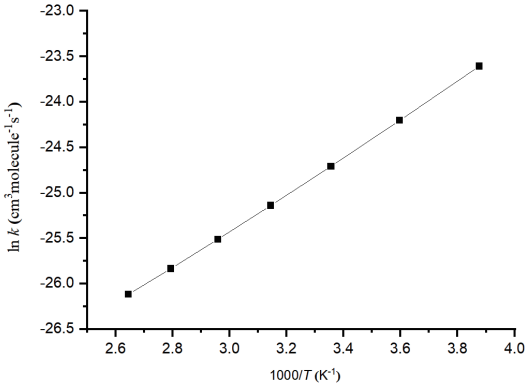

FIG. 4 Theoretically determined Arrhenius plot for M-BPR+HO_2 reaction over the 258–378 K temperature range at the CCSD(T)/cc-pVDZ//B3LYP/6-311G(d,p) level of theory.

The total rate constants for the M-BPR+HO_2 reaction are described by a Arrhenius three-parameter equation, as follows:

$$k(T) = 4.22 \times 10^{-15} \cdot \left(\frac{T}{300}\right)^{1.44} \cdot \exp\left(\frac{2505}{T}\right) \quad (2)$$

which provides a good fit of the rate constants calculated between 258 and 378 K. The positive exponential term of the three-parameter Arrhenius equation further confirms the negative temperature effect of the studied reaction.

The Arrhenius plot of the reaction is shown in FIG. 4, which clearly shows that the rate constants of the title reaction is negatively correlated with temperature over the temperature range studied. Generally, this

DOI: 10.1063/1674-0068/cjcp2407101

means that the M-BPR + HO_2 reaction should have at least one pathway with an energy barrier that is lower than the energy of the reactants [47]. Indeed, the calculated barrier height for M-BPR-^{3}TS1 (−4.67 kcal/mol) in the triplet pathway are lower than that of reactants at the CCSD(T)/cc-pVDZ//B3LYP/6-311G(d,p) level of theory. The total rate constant also shows a negative temperature dependence, since the total rate constant for the M-BPR + HO_2 reaction depends on the rate constant for the triplet state reaction.

IV. CONCLUSION

The reaction mechanism, thermodynamic parameters and kinetic analysis of the M-BPR + HO_2 reaction have been investigated in the present work. The triplet state of the reaction is shown to have only one reaction pathway which is the generation of hydroperoxide and $^3O_2$ via hydrogen abstraction, while there are four different reaction pathways for the singlet state, *i.e.*, the generation of other different products (*e.g.*, $^1O_2$, O_3, HO_2, OH, and HO_3H) via direct the hydrogen abstraction and addition-elimination reaction mechanism. From an energetic point of view, the triplet reaction has a lower barrier height (−4.67 kcal/mol), in contrast, the other four reaction channels of the singlet states have higher barriers heights and are less likely to occur. The rate constants of the M-BPR + HO_2 reaction were further studied over the temperature range 258–378 K, showing negative temperature dependence. The kinetic calculations indicate that the formation of the $C_8H_{11}O_2H + {}^3O_2$ channel is the most kinetically favourable, since its rate constants is at least seven orders of magnitude larger than that of the other channels in the temperature range studied. In addition, the positive exponential term of Arrhenius three-parameter equation implies a negative temperature dependence, confirming the negative temperature effect of the theoretical rate constants.

Supplementary materials: The mechanistic diagram of the *m*-Xylene-OH reaction system, the Cartesian coordinates of key molecules, and the values of the electronic energy and zero-point corrections of all the stationary points of M-BPR+HO_2 reaction are shown.

V. ACKNOWLEDGEMENTS

We would like to thank financial support from the Anhui University of Traditional Chinese Medicine High Level Talent Support Program Project (No.2021rcyb 01), the National Natural Science Foundation of China (No.42075113, No.91544228), Scientific Research Program of Higher Education Institutions in Anhui Province (2023AH050836).

[1] A. Mozaffar and Y. L. Zhang, Curr. Pollut. Rep. **6**, 250 (2020).
[2] K. Tsigaridis and M. Kanakidou, Atmos. Chem. Phys. **3**, 1849 (2003).
[3] K. P. Wyche, P. S. Monks, A. M. Ellis, R. L. Cordell, A. E. Parker, C. Whyte, A. Metzger, J. Dommen, J. Duplissy, A. S. H. Prevot, U. Baltensperger, A. R. Rickard, and F. Wulfert, Atmos. Chem. Phys. **9**, 635 (2009).
[4] C. Bloss, V. Wagner, A. Bonzanini, M. E. Jenkin, K. Wirtz, M. Martin-Reviejo, and M. J. Pilling, Atmos. Chem. Phys. **5**, 623 (2005).
[5] C. Bloss, V. Wagner, M. E. Jenkin, R. Volkamer, W. J. Bloss, J. D. Lee, D. E. Heard, K. Wirtz, M. Martin-Reviejo, G. Rea, J. C. Wenger, and M. J. Pilling, Atmos. Chem. Phys. **5**, 641 (2005).
[6] P. J. Ziemann and R. Atkinson, Chem. Soc. Rev. **41**, 6582 (2012).
[7] B. Bohn and C. Zetzsch, Phys. Chem. Chem. Phys. **14**, 13933 (2012).
[8] D. K. Henze, J. H. Seinfeld, N. L. Ng, J. H. Kroll, T. M. Fu, D. J. Jacob, and C. L. Heald, Atmos. Chem. Phys. **8**, 2405 (2008).
[9] A. Akherati, Y. C. He, M. M. Coggon, A. R. Koss, A. L. Hodshire, K. Sekimoto, C. Warneke, J. de Gouw, L. Yee, J. H. Seinfeld, T. B. Onasch, S. C. Herndon, W. B. Knighton, C. D. Cappa, M. J. Kleeman, C. Y. Lim, J. H. Kroll, J. R. Pierce, and S. H. Jathar, Environ. Sci. Technol. **54**, 8568 (2020).
[10] M. Asadi and M. Mirmohammadi, Environ. Qual. Manag. **27**, 83 (2017).
[11] P. F. Liu, N. Abdelmalki, H. M. Hung, Y. Wang, W. H. Brune, and S. T. Martin, Atmos. Chem. Phys. **15**, 1435 (2015).
[12] W. Y. Sun, A. Hamadi, F. E. C. Ardila, S. Abid, N. Chaumeix, and A. Comandini, Combust. Flame **244**, 112247 (2022).
[13] S. Saarikoski, H. Hellén, A. P. Praplan, S. Schallhart, P. Clusius, J. V. Niemi, A. Kousa, T. Tykkä, R. Kouznetsov, M. Aurela, L. Salo, T. Rönkkö, L. M. F. Barreira, L. Pirjola, and H. Timonen, Atmos. Chem. Phys. **23**, 2963 (2023).
[14] D. Srivastava, W. R. Li, S. R. Tong, Z. B. Shi, and R. M. Harrison, Chemosphere **334**, 139002 (2023).
[15] S. S. Pan and L. M. Wang, J. Phys. Chem. A **118**,

10778 (2014).
[16] R. Atkinson, Chem. Rev. **86**, 69 (1986).
[17] S. Toby, L. J. Van de Burgt, and F. S. Toby, J. Phys. Chem. **89**, 1982 (1985).
[18] R. Atkinson and J. Arey, Polycyclic Aromat. Compd. **27**, 15 (2007).
[19] Q. Zhang, Y. F. Xu, and L. Jia, Atmos. Chem. Phys. **19**, 15007 (2019).
[20] J. W. Fan and R. Y. Zhang, J. Phys. Chem. A **112**, 4314 (2008).
[21] S. Y. He, Y. Liu, M. D. Song, X. Li, S. H. Lu, T. Z. Chen, Y. J. Mu, S. R. Lou, X. D. Shi, X. H. Qiu, T. Zhu, and Y. H. Zhang, Environ. Sci. Technol. **57**, 20657 (2023).
[22] S. S. Pan and L. M. Wang, Acta Phys. -Chim. Sin. **31**, 2259 (2015).
[23] N. L. Ng, J. H. Kroll, A. W. H. Chan, P. S. Chhabra, R. C. Flagan, and J. H. Seinfeld, Atmos. Chem. Phys. **7**, 3909 (2007).
[24] P. Hohenberg and W. Kohn, Phys. Rev. **136**, B864 (1964).
[25] K. Raghavachari, G. W. Trucks, J. A. Pople, and M. Head-Gordon, Chem. Phys. Lett. **157**, 479 (1989).
[26] W. Kohn and L. J. Sham, Phys. Rev. **140**, A1133 (1965).
[27] C. Lee, W. T. Yang, and R. G. Parr, Phys. Rev. B **37**, 785 (1988).
[28] L. Q. Deng and T. Ziegler, Int. J. Quantum Chem. **52**, 731 (1994).
[29] S. Maeda, Y. Harabuchi, Y. Ono, T. Taketsugu, and K. Morokuma, Int. J. Quantum Chem. **115**, 258 (2015).
[30] B. Long, J. L. Bao, and D. G. Truhlar, J. Am. Chem. Soc. **141**, 611 (2019).
[31] B. Long, J. L. Bao, and D. G. Truhlar, J. Am. Chem. Soc. **138**, 14409 (2016).
[32] B. Long, X. F. Tan, Z. W. Long, Y. B. Wang, D. S. Ren, and W. J. Zhang, J. Phys. Chem. A **115**, 6559 (2011).
[33] M. J. Frisch, G. W. Trucks, H. B. Schlegel, G. E. Scuseria, M. A. Robb, J. R. Cheeseman, G. Scalmani, V. Barone, G. A. Petersson, H. Nakatsuji, X. Li, M. Caricato, A. V. Marenich, J. Bloino, B. G. Janesko, R. Gomperts, B. Mennucci, H. P. Hratchian, J. V. Ortiz, A. F. Izmaylov, J. L. Sonnenberg, D. Williams-Young, F. Ding, F. Lipparini, F. Egidi, J. Goings, B. Peng, A. Petrone, T. Henderson, D. Ranasinghe, V. G. Zakrzewski, J. Gao, N. Rega, G. Zheng, W. Liang, M. Hada, M. Ehara, K. Toyota, R. Fukuda, J. Hasegawa, M. Ishida, T. Nakajima, Y. Honda, O. Kitao, H. Nakai, T. Vreven, K. Throssell, J. A. Montgomery Jr, J. E. Peralta, F. Ogliaro, M. J. Bearpark, J. J. Heyd, E. N. Brothers, K. N. Kudin, V. N. Staroverov, T. A. Keith, R. Kobayashi, J. Normand, K. Raghavachari, A. P. Rendell, J. C. Burant, S. S. Iyengar, J. Tomasi, M. Cossi, J. M. Millam, M. Klene, C. Adamo, R. Cammi, J. W. Ochterski, R. L. Martin, K. Morokuma, O. Farkas, J. B. Foresman, and D. J. Fox, *Gaussian 16, Revision A.03*, Wallingford: Gaussian Inc., (2009).
[34] H. J. Werner, P. J. Knowles, G. Knizia, F. R. Manby, and M. Schütz, WIREs. Comput. Mol. Sci. **2**, 242 (2012).
[35] H. J. Werner, P. J. Knowles, F. R. Manby, M. Schütz, P. Celani, G. Knizia, T. Korona, R. Lindh, A. Mitrushenkov, G. Rauhut, T. B. Adler, R. D. Amos, A. Bernhardsson, A. Berning, D. L. Cooper, M. J. O. Deegan, A. J. Dobbyn, F. Eckert, E. Goll, C. Hampel, A. Hesselmann, G. Hetzer, T. Hrenar, G. Jansen, C. Köppl, Y. Liu, A. W. Lloyd, R. A. Mata, A. J. May, S. J. McNicholas, W. Meyer, M. E. Mura, A. Nicklass, P. Palmieri, K. Pflüger, R. Pitzer, M. Reiher, T. Shiozaki, H. Stoll, A. J. Stone, R. Tarroni, T. Thorsteinsson, M. Wang, and A. Wolf, *Molpro, version 2010.1, A package of ab initio programs*, (2010).
[36] H. Eyring, J. Chem. Phys. **3**, 107 (1935).
[37] M. G. Evans and M. Polanyi, Trans. Faraday Soc. **31**, 875 (1935).
[38] D. G. Truhlar, B. C. Garrett, and S. J. Klippenstein, J. Phys. Chem. **100**, 12771 (1996).
[39] C. Eckart, Phys. Rev. **35**, 1303 (1930).
[40] W. T. Duncan, R. L. Bell, and T. N. Truong, J. Comput. Chem. **19**, 1039 (1998).
[41] M. J. Elrod, J. Phys. Chem. A **115**, 8125 (2011).
[42] S. N. Wang, R. R. Wu, T. Berndt, M. Ehn, and L. M. Wang, Environ. Sci. Technol. **51**, 8442 (2017).
[43] A. W. Birdsall and M. J. Elrod, J. Phys. Chem. A **115**, 5397 (2011).
[44] W. Hua, Z. M. Chen, C. Y. Jie, Y. Kondo, A. Hofzumahaus, N. Takegawa, C. C. Chang, K. D. Lu, Y. Miyazaki, K. Kita, H. L. Wang, Y. H. Zhang, and M. Hu, Atmos. Chem. Phys. **8**, 6755 (2008).
[45] A. M. Thompson, Science **256**, 1157 (1992).
[46] M. Lee, B. G. Heikes, and D. W. O'Sullivan, Atmos. Environ. **34**, 3475 (2000).
[47] H. Hou, J. C. Li, X. L. Song, and B. S. Wang, J. Phys. Chem. A **109**, 11206 (2005).

DOI: 10.1063/1674-0068/cjcp2407101